Diagnostic modeling of the shoreline variation along the Jiangsu Coast, China

Kuai, Yu; Aarninkhof, Stefan; Wang, Zheng Bing

DOI
10.1016/j.geomorph.2023.108581

Publication date
2023

Document Version
Final published version

Published in
Geomorphology

Geomorphology 425 (2023) 108581

Contents lists available at ScienceDirect

Geomorphology

journal homepage: www.journals.elsevier.com/geomorphology

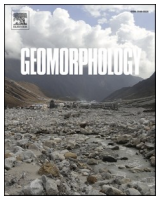

Diagnostic modeling of the shoreline variation along the Jiangsu Coast, China

Yu Kuai [a,*], Stefan Aarninkhof [a], Zheng Bing Wang [a,b]

[a] Faculty of Civil Engineering and Geosciences, Delft University of Technology, 2628 CN Delft, the Netherlands
[b] Deltares, 2600 MH Delft, the Netherlands

ARTICLE INFO

Keywords:
Intertidal flat
Beach slope
Sediment grain-size
Bed composition
Jiangsu Coast

ABSTRACT

Intertidal flats are of great socio-economic and ecological importance in defending the coastal cities from flooding, providing resources for land reclamations and habits for wildlife. On the intertidal flats, milder profiles are usually featured with finer sediment. However, we find the opposite relationship between the alongshore variation in intertidal slope and sediment grain size on the intertidal flat along the Jiangsu Coast. With a conceptual figure of the hydrodynamics and shoreline evolution on this coast, we hypothesize that the unexpected pattern is caused by the alongshore gradient in hydrodynamic forcing. In order to test our hypothesis, we carry out a series of numerical model simulations in a highly schematized manner to investigate the real mechanism behind this unexpected pattern. Through the analysis, we find that only the southwards coarsening pattern is inconsistent with the shoreline evolution pattern. This inconsistency is not induced by alongshore hydrodynamic gradient, and can only be explained by different sediment provenances. We also find that the alongshore shoreline evolution pattern is not only determined by the alongshore gradient in hydrodynamic forcing, but also influenced by the alongshore variation in bed composition. In the erosion/sedimentation transition zone, the bed composition factor plays the major role.

1. Introduction

Intertidal flats are normally formed in fine-sediment-rich environment, where tides dominate over wind waves (Friedrichs, 2012; Gao, 2019). The intertidal flats serve as a vital component in land- ocean interactions. They are of great socio-economic and ecological importance in defending the coastal cities from flooding, providing resources for land reclamations and habits for wildlife (Reed et al., 2018; Muller et al., 2020; Chen et al., 2021). In order to comprehensively manage the coastal engineering and maintain the ecosystem in a more effective and sustainable way, it is crucial to understand the intertidal flat morphodynamics and physical processes.

Tide is considered to be the most dominant force in determining the existence of the intertidal flats (Le Hir et al., 2000; Pritchard et al., 2002). Tidal current can normally be split into a cross-shore component and an alongshore one, and the relative importance of these two components depends on the large-scale circulation around the flat (Le Hir et al., 2000). The cross-shore tidal current is often considered to be responsible for shaping the profile. Therefore, the intertidal flat is usually schematized into a one-dimensional cross-shore profile in previous studies to investigate its morphological and sedimentary characteristics (Roberts et al., 2000; Pritchard et al., 2002; Pritchard and Hogg, 2003; Liu et al., 2011; Maan et al., 2015; Zhou et al., 2015). The contribution of the other natural processes to the evolution of intertidal flats has also been studied, such as wind waves (Green and Coco, 2007; Zhou et al., 2015), and sediment supply (Liu et al., 2011; Zhou et al., 2015). By driving a one-dimensional model with different combinations of tidal range, wave climate and sediment supply, Liu et al. (2011) found that the width of equilibrium intertidal flat is positively related to tidal range with invariant sediment supply, and increasing sediment supply leads to wider intertidal flats. The intertidal flats in straight shorelines exhibit the convex-up shape in the tide-dominant environment and the concave-up shape in case of wave dominance, respectively (Roberts et al., 2000). The intertidal flat sedimentation zonation generally presents a shoreward fining pattern (Alexander et al., 1991; Whitehouse et al., 2000; Kuai et al., 2021), and this zonation is influenced by the tidal currents, wind waves, sediment properties and sediment supply as well (Zhou et al., 2015).

However, the contribution of alongshore currents to the intertidal sediment transport has also been addressed (Wang et al., 2006; Gong

* Corresponding author.
E-mail address: y.kuai@tudelft.nl (Y. Kuai).

https://doi.org/10.1016/j.geomorph.2023.108581
Received 7 July 2022; Received in revised form 30 December 2022; Accepted 1 January 2023
Available online 12 January 2023

et al., 2012; Wang et al., 2019b). The alongshore currents enhance the bed shear stress and stimulate the re-suspension of surficial sediments. This alongshore gradient can also lead to the alongshore variation of the intertidal flat morphology and sedimentology.

In our previous field data study (Kuai et al., 2021), we found several morphological and sediment distributions patterns on the Jiangsu Coast, China (Fig. 1), a typical tide-dominated muddy open coast with significant alongshore tidal current.

1. In the cross-shore direction, sediment tends to be finer landward in the intertidal zone. The same phenomenon was found at many muddy environment, like the Skeffling mudflat inside the mouth of Humber estuary (Whitehouse et al., 2000), the northern intertidal flat of the Seine estuary (Le Hir et al., 2000), and the central west coast of Korea (Alexander et al., 1991). This is opposite to wave-dominated sandy beaches where the coarsest sediment is near shoreline (Elfrink and Baldock, 2002).
2. In the alongshore direction:
   a. The intertidal beach slope in the eroding northern coast is larger than that in the accreting southern coast, and the eroding profiles tend to be concave up and the accreting ones are more convex up. Similar pattern was also observed on the tidal flats in the northern coast of the Gulf of Tonkin, Vietnam (Tong et al., 2020). The tidal flats in the San Francisco Bay were also found to be concave up under erosion conditions, while convex up under sedimentation conditions (Bearman et al., 2010).
   b. In the accreting southern coast, while tidal flat slopes are generally becoming milder towards the south, the corresponding bed surface sediment grain size is becoming coarser southward (Fig. 2). This is opposite to the findings on other tidal flats where the milder tidal flats have finer bed materials, like the tidal flats in the San Francisco Bay (Bearman et al., 2010) and the mudflat on the eastern coast of the Ariaka Bay, Japan (Yamada and Kobayashi, 2004).
3. In the eroding northern coast, we found alternating patterns of very fine and coarse sediment (depending on the local clay content). The same pattern was also found in the Mekong Delta (Gugliotta et al., 2019). This pattern was attributed to the occurrence of two different erosion resistant mechanisms, viz. self-weight consolidation and armoring effect (Fig. 3), when the flat erodes to an erosion resistant layer (Kuai et al., 2021).

The observed morphological and sediment distribution patterns on the Jiangsu Coast are similar to other tide-dominant muddy flats, except the relationship between alongshore beach slope variation and sediment grain size pattern, which is totally opposite to these flats. This paper is aimed to explain the mechanism behind the alongshore variation of beach slope and remarkable sediment grain size along the Jiangsu intertidal flats. To that end, we formulate a conceptual figure with special focus on describing the alongshore variations in hydrodynamics and shoreline evolution pattern. Based on the conceptual figure, a highly schematized Delft3D numerical model is set up, with which we investigate the sediment transport pattern at different alongshore transects driven by tides and waves. By comparing the sediment transport rates along different transects, we get the erosion/sedimentation pattern in-between these transects and validate that with the shoreline evolution history. With further analysis of simulated sediment transport pattern of different fractions, we deepen our insight into the mechanisms that can explain the observed alongshore distribution of sediment grain sizes at the intertidal beach.

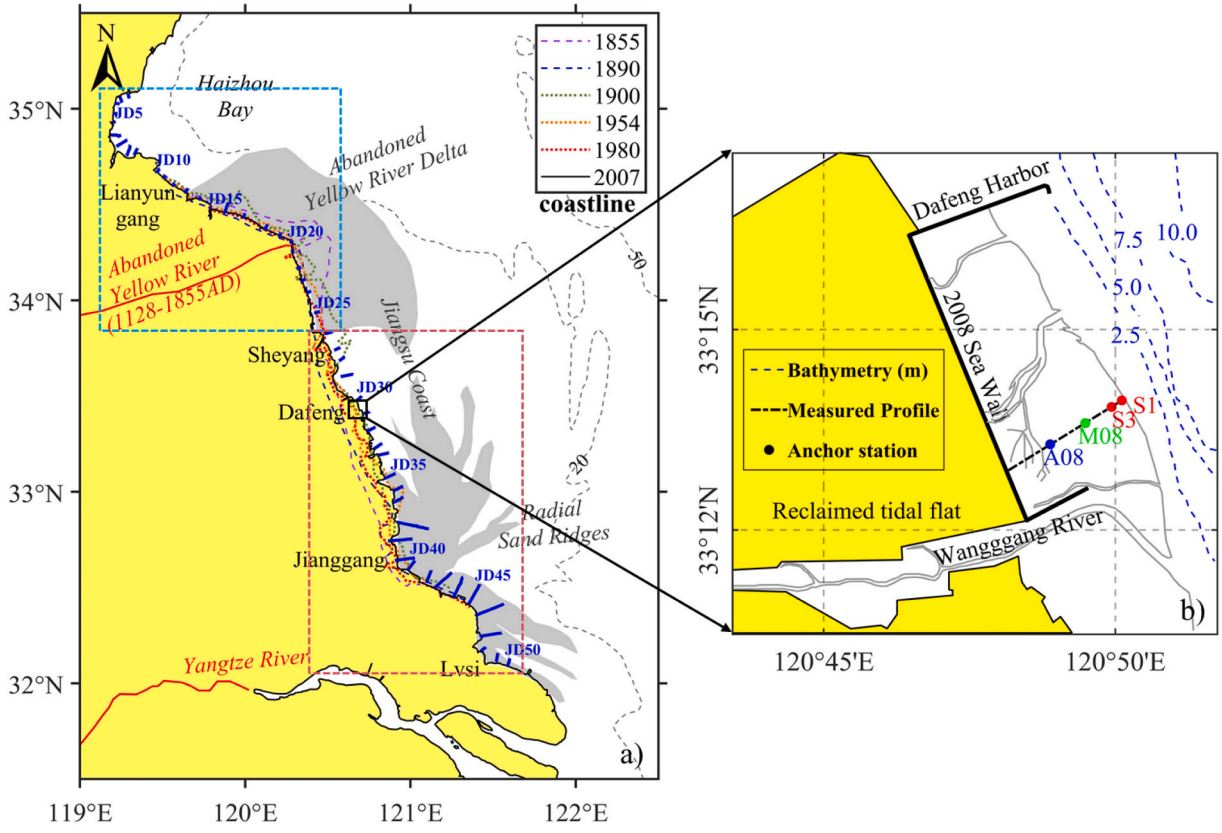

Fig. 1. Overview of the Jiangsu Coast. a) Shoreline evolution of the Jiangsu Coast (adapted from Su et al., 2017) and measured profiles location (marked with blue short solid lines). The blue and red dash rectangular indicate the eroding northern and accreting southern coast, respectively. b) The site of field measurements in Dafeng in 2008: A08, M08, and S1/S3 are anchor stations for hydrodynamic and sediment concentration measurements (adapted from Wang et al., 2012b).

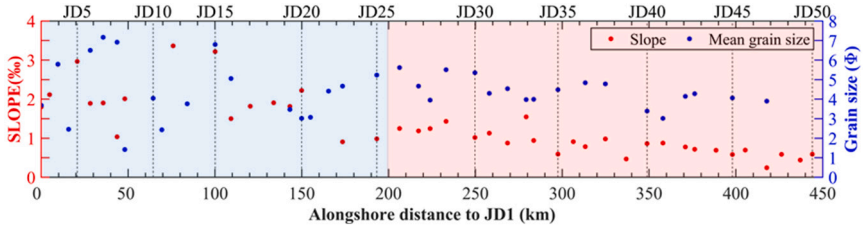

Fig. 2. Alongshore distribution of intertidal beach slope and mean grain size of the surficial sediments. Blue and red shades indicate the eroding and accreting part of the coast as shown in Fig. 1. Dash lines represent the location of every 5 measured profiles.

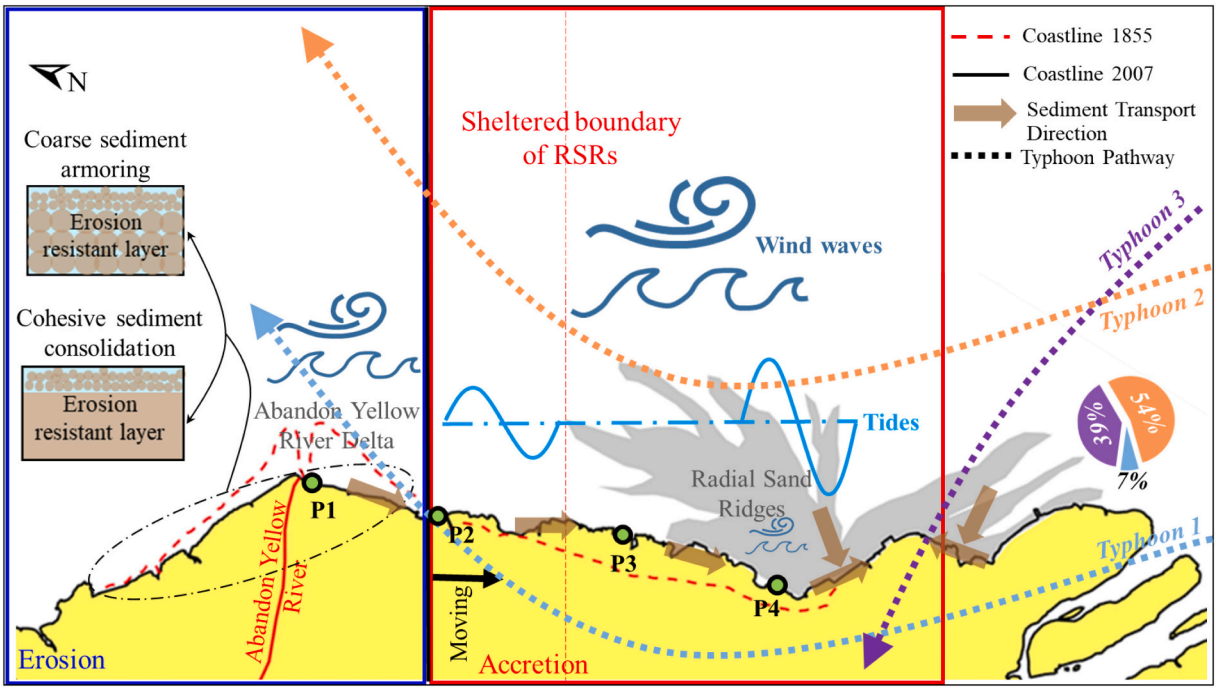

Fig. 3. A conceptual figure of the Jiangsu Coast dynamic processes including shoreline evolution, general nearshore sediment transport direction of the Jiangsu coast, tidal amplitude distribution, wind waves sheltering conditions and ~ 50 years (1949– 2007) typhoon pathways and frequency (pie chart).

2. Methods

2.1. Conceptual figure of the Jiangsu Coast

Kuai et al. (2021) provides a detailed overview of the hydrodynamics and morphology of the Jiangsu Coast. Based on those findings, we formulate a conceptual figure that breaks up the Jiangsu coast in four different sections, namely P1 ~ P4, characterized by similar shoreline evolution and hydrodynamics (Fig. 3). P1 is near the top of the Abandoned Yellow River Delta (AYRD), P2 is near the transition boundary between erosion and accretion shoreline, P3 is at the north part of the sheltered coast and P4 is near the central of the Radial Sand Ridges (RSRs). The northern Jiangsu coast is under erosion while the southern part is still accreting. Meanwhile the transition boundary between the two parts is gradually moving southwards (Zhang et al., 2002). The eroded fine sediment from the north part partly transports along the coastline towards the south and eventually settles there. Apart from the feeding from the northern coast, the intertidal beach on the southern coast also has great sediment exchange with the offshore RSRs. The tidal wave propagates parallel to the coastline in the nearshore zone. The mean tidal range increases from ~2 m at the AYRD to ~6 m near the center of the RSRs (Wang et al., 2019a). Due to the sheltering effect of the RSRs, the wave energy in the sheltered zone is smaller than that in the exposed area. Overall, according to the ~50 years meteorological record (from 1949 to 2007), there are 76 typhoons that influenced the Jiangsu Coast, of which only 5 (~7 %) landed on the Jiangsu Coast or the Yangtze Estuary (Typhoon1 in Fig. 3). On the one hand, the frequency of storm surges can be considered minor compared to the continuous sediment reworking by tidal currents and normal wind waves; On the other hand, they usually only last 1–2 days with a maximum significant wave height of ~2 m at the nearshore zone (Gong et al., 2019a) and the tidal flats are under a 'storm surges destroy - tidal currents restore' cycle (Zhang et al., 1998; Gong et al., 2019b). According to the existing model study (Pu et al., 2022), the net sediment transport caused by the northerly winds (representing winter storms) is comparable to that of the southerly winds (representing typhoons). Therefore, although winter storms and typhoons can drive massive sediment transport in a short period, their contribution to annual sediment transport is limited. In this study, we focus on the annual evolution of the beach, and the temporal influence of storm surges is not investigated in line with other studies (Xing et al., 2012; Xu et al., 2016).

Based on this conceptual figure, we hypothesize that the observed alongshore variations in morphology and sedimentology (southward flattening of beach slopes, and coarsening of sediment grain size) can be explained by alongshore gradients in hydrodynamic forcing (variations in tidal amplitude, alongshore vertical tide phase variation, and wave sheltering in lee side of RSRs). We will test these hypotheses with a simple, 1D process-based model applied to a few characteristic, cross-

shore transects along the Jiangsu coast.

2.2. Numerical model

In order to investigate the impact of alongshore variations in the hydrodynamic forcing, we carry out morphological simulations for different, representative parts of the coastline. We do so with a highly schematized model using the DELFT3D software (Lesser et al., 2004), assuming hydrodynamic processes (tides, waves) to be uniform within a short distance alongshore (~10 km). Under this assumption, the coast is divided into several sections, namely P1 ~ P4 in the conceptual figure (Fig. 3), based on the local hydrodynamic conditions (in terms of tidal amplitude, alongshore vertical tidal phase variation and wave climate). Each section is schematized with a rectangular domain and an alongshore uniform initial bathymetry. These sections have different initial intertidal slope and the same initial bed sediment composition.

The model domain is 10 km in both cross-shore and alongshore directions (Fig. 4). The grid size is 100 m in cross-shore direction and 400 m in alongshore direction. The initial bed elevation is set to be 2.5 m above Mean Sea Level (MSL) at the landward end of the model and linearly decreases to the seaward end based on the local intertidal beach slope. The threshold depths for drying / flooding and sediment transport computing are both set to be 0.05 m. A uniform Chezy coefficient of 65 $m^{1/2}/s$ is applied throughout the whole domain.

Three open boundaries are set, namely north, south and sea boundary. Since the purpose of the model is to compare the different transects, not to reproduce the accurate morphological evolution on each transect, we neglect the spring-neap variation in the tidal signal. we simplify the tidal signals into the M2 harmonic (as it is the most dominant harmonic in this region) to represent the mean tidal amplitudes at different locations. The M4 harmonic is also added in the model to represent tidal asymmetry. The M2 and M4 tides with a phase difference ($2\varphi M2-\varphi M4$) of -142° are prescribed at the lateral boundaries (North and South boundaries). Their amplitude and alongshore phase variation are set according to different local conditions. A Neumann boundary condition (Roelvink and Walstra, 2004) viz. zero cross-shore water level gradient is imposed at the seaward boundary.

Due to refraction, waves tend to be more or less perpendicular to the coastline when approaching the shallow zone. In the model, the wave is assumed to normally incident along the sea boundary with stationary wave parameters which are determined by the local situations and represent the year-round wave condition. A stationary wind field of 5 m/s is set to maintain the wave energy when it propagates landwards. The wind wave is online coupled with the flow during the simulation. There are only two nearshore wave stations along the Jiangsu coast (i.e., Lianyugang station and Lvsi station, see Fig. 6.e), which are insufficient to represent the wind/wave climate of the whole domain. Therefore, we consider the wave effect in a schematic manner, i.e., extracting the significant wave height for the schematized model from a large-scale model, which is driven by stationary wind and wave conditions.

The bed material is schematized into three sediment fractions, namely clay, silt and sand. The clay and silt are treated as cohesive sediment and the sand is treated as non-cohesive sediment, and the sediment property parameters are listed in Table 1. The widely adopted Partheniades-Krone formulations (Partheniades, 1965) and Engelund-Hansen formulations (Engelund and Hansen, 1967) are used for cohesive and non-cohesive sediment respectively. Because there is no such measured data introducing the detailed Suspended Sediment Concentration (SSC) of each sediment fraction along a cross-shore profile at different alongshore locations, it is difficult to get the accurate SSC boundary conditions for different alongshore location. The general measured cross-shore SSC distribution pattern at the Jiangsu Coast shows that the SSC can reach more than 1 kg/m^3 on the tidal flat and decreases to less than 0.5 kg/m^3 at 20 km offshore (Ren, 1986; Xu et al., 2016; Wang et al., 2019b). In our model, we set the boundary SSC the same value for different locations. On lateral boundaries, the SSC is set to decrease linearly from 1.25 kg/m^3 at the landward edge to 0.75 kg/m^3 at the seaward end. The ratio between SSC of clay and silt is 1:4. The initial bed is composed of 10 m well mixed sediments, and the detailed composition of each fraction adopts an existing filed data set collected

Table 1
Sediment properties in the model setting (ρ_D is the dry bed density, T_{cr} is the critical bed shear stress for erosion, W_0 and Ws are the fresh and saline settling velocity respectively, M is the erosion parameter and D_{50} is the medium grain diameter).

Sediment ID	ρ_D (kg/m^3)	T_{cr} (pa)	W_0 (mm/s)	W_s (mm/s)	M (kg/m^2/s)	D_{50} (um)
Clay	1000	0.1	0.1	0.5	0.0002	0.5
Silt	1000	0.2	0.2	0.5	0.0002	25
Sand	1600	–	–	–	–	100

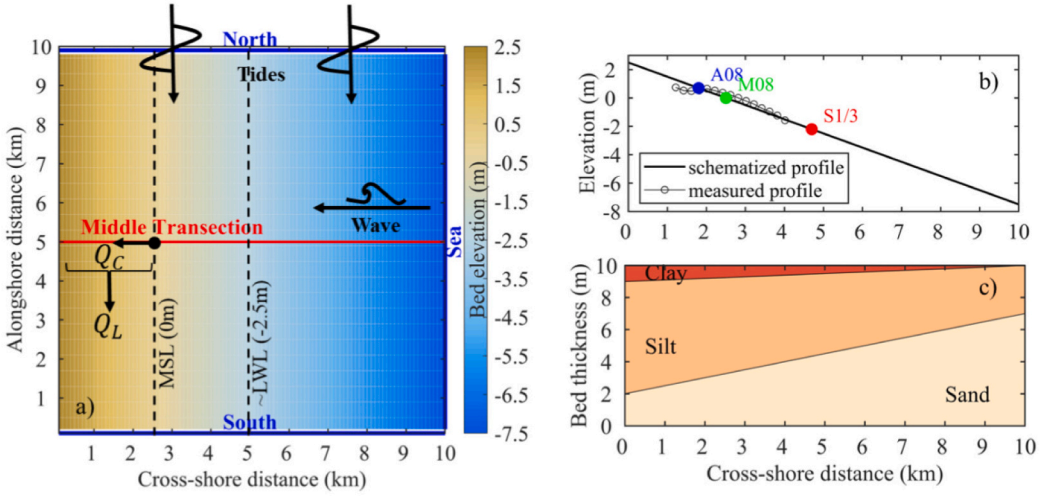

Fig. 4. Numerical model scheme set up. a) Grid and initial bathymetry of the schematized model (Middle transection is chosen as the monitoring profile; Three open boundaries are marked with blue solid lines; The mean sea level is set to be 0 m in this model) b) Measured and schematized cross-shore profile, and the location of monitoring points c) Initial bed composition of the Dafeng validation case based on the measured data from Wang et al. (2012b).

on the intertidal flat in Dafeng (Wang et al., 2012b, Fig. 1.b). According to this observation data, from landward end to seaward end, the clay proportion is decreasing from 10 % to 0 %, the silt proportion is decreasing from 70 % to 30 %, while the sand proportion is increasing from 20 % to 70 % (Fig. 4.c).

In order to test the reliability of the simplified model scheme as regards to hydrodynamics and sediment transport processes, we compare model results to the existing field data set in Dafeng (Wang et al., 2012b). In the verification run, we drive the model with tide and wave signals measured in Dafeng. The M2 and M4 tides are set to be 2 m and 0.2 m in amplitude, and the significant wave height and wave period are set to be 0.3 m and 2.5 s, respectively. Then we compare the model results between different sections (P1 ~ P4), and the hydrodynamic parameters for these sections are described in Chapter 2.4.

2.3. Model verification

The purpose of the model is to compare the sediment transport pattern between different transects. Therefore, the model needs to reproduce reliable sediment transport processes. We compare the simulated time series of water depth, cross-shore and alongshore depth-averaged velocities and SSC with the measurement in Dafeng. Three observation points namely A08, M08 and S1/3 are selected on the central profile of the model domain (Fig. 4.b), representing the upper, middle, and lower intertidal flat, respectively, which is consistent with the field measurement in Dafeng (Fig. 1.b).

The simulated variation of water depth agrees well with the measurement (Fig. 5). Since the measured variations are rather noisy due to the shallow water depth, our model adopts a simplified initial bathymetry and takes only two tidal components into account. It is difficult to compare the exact temporal variations of cross-shore velocity (V_c), alongshore velocity (V_l) and SSC between the simulated and measured results in a strictly point-by-point manner. Despite the model is highly simplified, the measured and simulated magnitudes of V_c, V_l and SSC match well with each other. As it can be seen from Fig. 5, the simulated peak flood/ebb velocity magnitude, flood/ebb duration, and maximum SSC agree well with the measured data. The verification results demonstrate that such model is capable of reproducing reliable sediment transport processes.

2.4. Hydrodynamic parameters

We couple the wind and wave to a well-validated Jiangsu Region tide model (Yao et al., 2018). The wind considered in the model is simplified with a NE ~ E direction and a speed of 4.5–5 m/s, which is similar to the existing model study (Su et al., 2017). The boundary wave force is set with a mean significant wave height of 1 m and mean period of 5 s to represent the yearly average situation, following the previous study (Chen et al., 2013b).

The tidal amplitude, alongshore phase gradient and significant wave height at the seaward end of each measured profile (location see Fig. 1) are extracted from the coupled Jiangsu Region tide and wave model results (Fig. 7). As it can be seen from Fig. 7, from JD 20 to JD40, the M2 tidal amplitude shows an increasing pattern, while its alongshore phase gradient shows a decreasing trend. The significant wave height slightly increases from JD 20 to JD 30, and then dramatically decreases southwards due to the sheltering effect of the RSRs (Fig. 7.b). The wave is getting perpendicular to the shoreline when it is approaching the

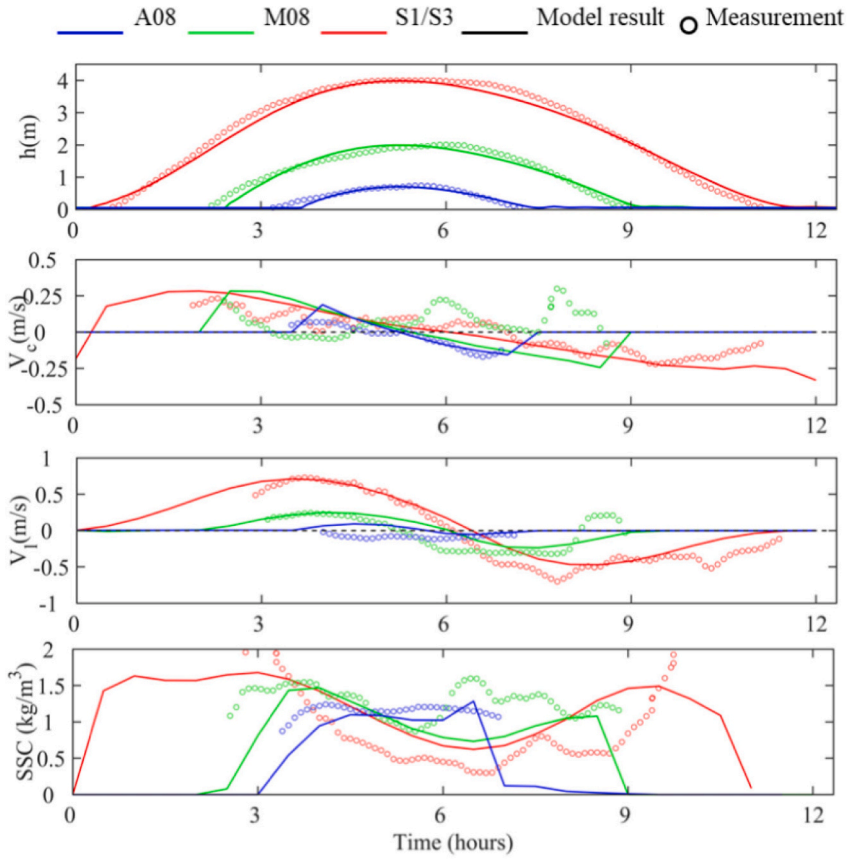

Fig. 5. Measured (circles) and modelled (solid lines) time series of water depth, depth-averaged velocity, and suspended sediment concentration measured at the upper (A08, blue line), middle (M08, green line), and lower (S1/S3, red line) intertidal flat. V_c and V_l are the current velocity components across (offshore [ebb] "-" and onshore [flood] "+") and along (northward [ebb] "-" and southward [flood] "+") the intertidal flat, respectively.

shallower zone (Fig. 6), which is consistent with the wave setting in our schematized model. The detailed hydrodynamic setting of the scenarios is shown in Table 2.

3. Results

3.1. Simulated sediment transport and shoreline evolution pattern

We calculate the net cross-shore (Q_C) and alongshore (Q_L) sediment transport rates during one M2 tidal cycle after 30 tidal cycles (Fig. 8). The Q_C is the tidal averaged cross-shore sediment transport rate at a certain depth, which means the net cross-shore sediment transport tendency at a certain point during one M2 tidal cycle. The Q_L is the tidal averaged alongshore sediment transport rate integrated from a certain depth to the most landward point, which means the net alongshore sediment transport tendency above a certain point during one M2 tidal cycle (Fig. 4.a). It can be seen from Fig. 8 that the Q_L is one order larger than the Q_C near the low water line (−2.5 m), while their magnitudes are similar at the mean sea level (0 m). This is mainly because the coast is an alongshore current dominant one, and the alongshore current is dominant over the cross-shore one in the lower intertidal flat. However, in the upper intertidal flat, the alongshore current is weak due to the limited water depth, and the current in two directions are of similar magnitude (see Fig. 5). This is consistent with other research on alongshore tidal current dominated flat (Wang et al., 2006; Gong et al., 2012; Wang et al., 2019b). We also found that the sediment transport rate near the low water line is more than one order larger as compared to that at the mean sea level. This is because the alongshore tidal currents are much larger at deeper water and waves are only of secondary importance.

Table 2
Tide, wave and initial slope conditions for different scenarios.

Scenario ID	Tidal boundary		Wave condition		Profile condition
	Amplitude (m)	Phase difference (°)	Tp (s)	Hsig (m)	slope (‰)
P1	M2:0.83 M4:0.17	M2:11.75 M4:9.68	3.0	0.52	2.0
P2	M2:1.15 M4:0.18	M2:7.65 M4:11.90	2.9	0.58	1.2
P3	M2:1.74 M4:0.20	M2:5.40 M4:11.26	2.7	0.4	1.0
P4	M2:1.92 M4:0.39	M2:4.05 M4:16.11	2.0	0.18	0.9

The simulated net onshore sediment transport rate generally shows a southward increasing pattern, except for the slightly decreasing trend between P3 and P4 (Fig. 8). This is because the tidal range increases towards the south in this tide-dominant environment. Although wave is only of secondary importance, the sheltering effect of the RSRs makes the wave dynamic much weaker in P4 than it in P3 (Table 2). In P3, the enhanced bed shear stress by waves leads to more resuspension and hence larger sediment transport rate. The southward increasing net onshore transport pattern indicates that more sedimentation on the intertidal flat to the south by cross-shore sediment transport. However, its magnitude is much smaller compared to the alongshore sediment transport induced shoreline evolution.

The simulated net alongshore sediment transport rate shows an increasing trend from P1 to P3, and a decreasing trend from P3 to P4 (Fig. 8). By looking at the gradient of the alongshore sediment transport

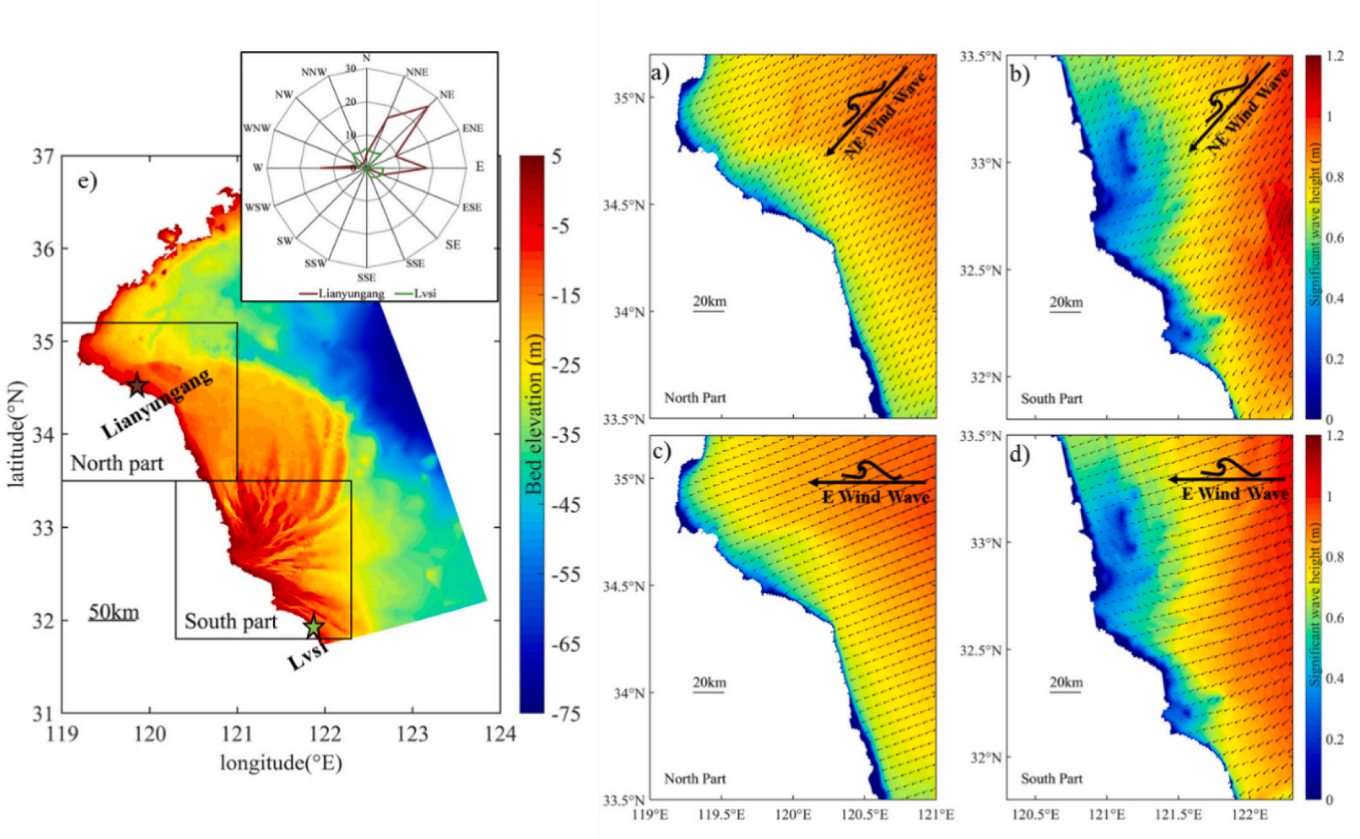

Fig. 6. Simulated wave energy distribution with different incident wind wave directions. a) and b) represent the results of NE incident wind wave. c) and d) represent the results of E incident wind wave. The colors indicate the significant wave height, and the arrows denote the mean wave direction. e) indicates the bathymetry of the modelled domain, and the frequency distribution of wave directions at two stations: Lianyungang (in red) and Lvsi (in green). Different circles denote different levels of concurrency frequency.

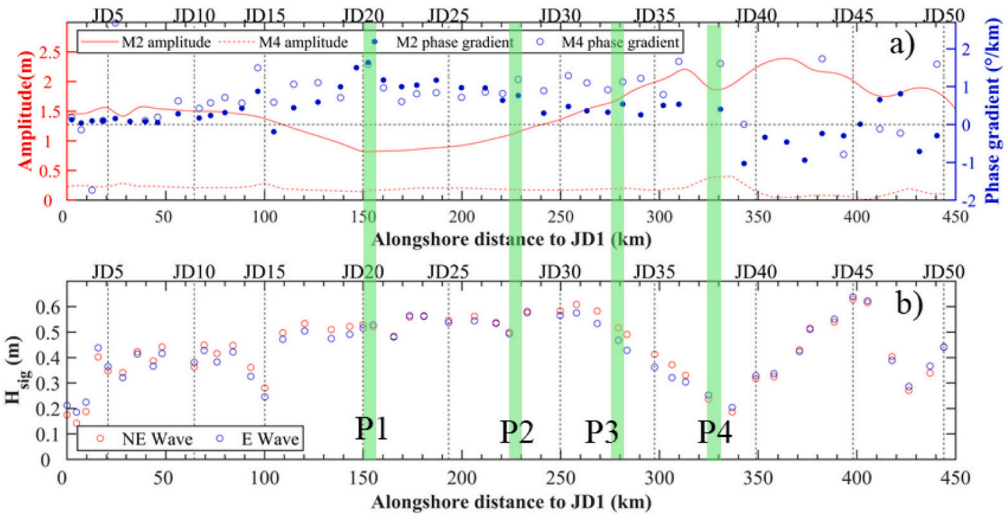

Fig. 7. a) Alongshore distribution of M2 and M4 tide properties derived from the Fourier analysis of a large scale Jiangsu Coast tide model (Yao et al., 2018). The red lines indicate the amplitude and the blue dots and circles indicate the alongshore tidal phase gradient. b) Alongshore distribution of the significant wave height at seaward end of each measured profile. Red circles represent the result of NE wind waves and the blue circles represent the results of E wind waves. Green bars indicate the profile data adapted for scenario (namely P1 ~ P4) simulations.

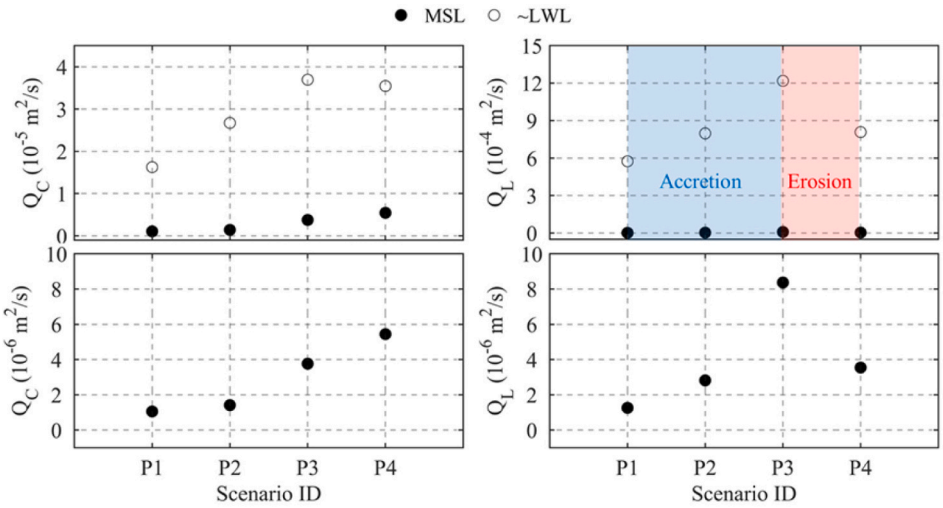

Fig. 8. Simulated net suspended sediment transport rate during one M2 tidal cycle, the left panels are the cross-shore component (positive value means onshore transport), and the right panels are the alongshore component (positive means southward transport). The lower two panels are zoom in on the upper panels in the range of 0– 10 × 10^{-6} m^2/s. Black dots represent the results calculated at mean sea level (0 m in the model domain), and black circles represent the results calculated near the low water line (−2.5 m in the model domain).

between these four sections, we can get the shoreline evolution tendency in-between these sections. The coastline is experiencing severe erosion between P1 and P2, P2 and P3, and notable accretion between P3 and P4. This pattern is not fully consistent with the shoreline evolution history (Fig. 3). In the conceptual figure, P2 is chosen near the erosion and deposition boundary of the coastline, which means the coastline between P2 and P3 should be experiencing mild sedimentation.

The inconsistency of the shoreline evolution condition between P2 and P3 proves that we cannot get the proper alongshore pattern of morphological changes by only taking the alongshore gradient in hydrodynamic forcing into account. We discuss the influence of initial bed composition setting on model results in Section 3.3.

3.2. Simulated transport of different sediment compositions

In order to interpret the sediment grain size alongshore variation pattern, we further calculate the contribution of each sediment fraction to the total net cross-shore and alongshore transport. The transport proportions of each fraction are listed in Tables 3 and 4. By comparing the transport of each fraction between different sections, we investigate how the bed grain size evolves under the alongshore varying hydrodynamic forcing.

As it can be seen from the Tables 3 and 4, the net cross-shore transport rate proportion of each sediment fraction (clay, silt and sand) keeps more or less the same among different transects. The alongshore difference of the net cross-shore transport rate proportion is less than 0.5 %.As a consequence, the cross-shore transport process is considered to be minor importance to the observed alongshore variation in sediment grain size.

In the alongshore direction, the alongshore variation of the relative contribution of these three sediment fractions shows similar pattern to the cross-shore transport. However, difference between transects is much larger, especially near the mean sea level. Towards the south, the relative contribution of the fine material (clay) to the net southward alongshore sediment transport is decreasing around 5 %, while the relative contribution of the coarser materials (silt or sand) is increasing.

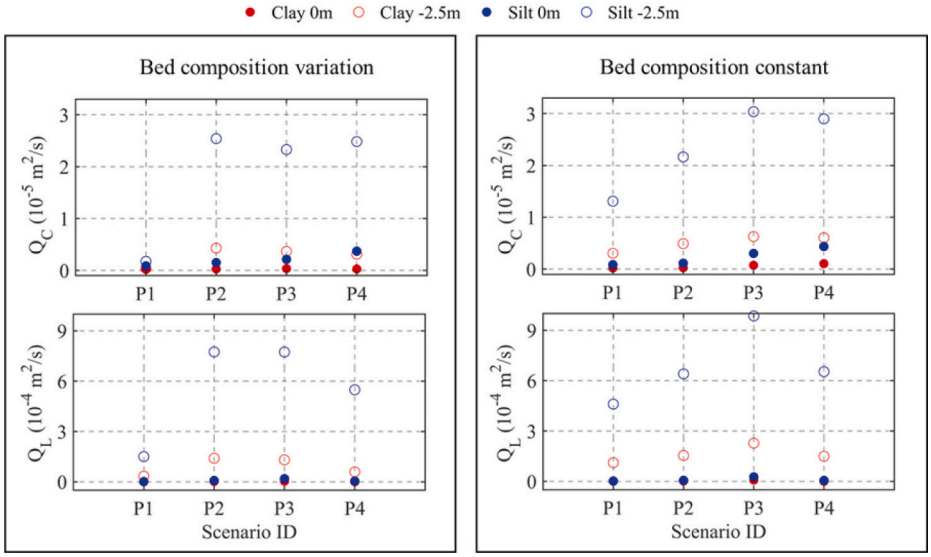

Fig. 9. Modelled net suspended sediment transport rate during one tidal cycle. The left panel shows results with bed composition applying measured data, and the right panel shows results with the same bed composition for all profiles.

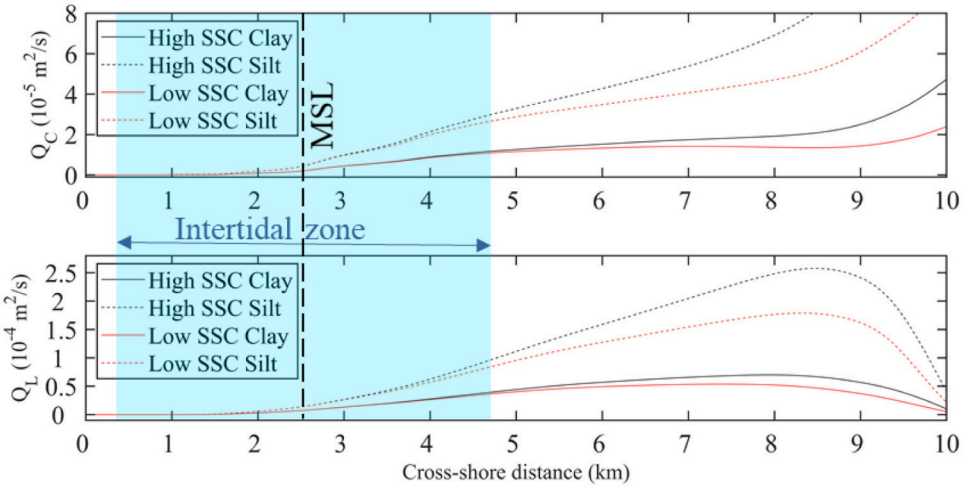

Fig. 10. Sensitivity of the sediment transport rate to the SSC boundary conditions. Light blue shadow marks the intertidal location, vertical black dash line indicates the location of mean seal level.

Table 3
Net sediment transport rate proportion of each fraction at 0 m.

Mean sea level	Sediment ID	Transport rate proportion (%)			
		P1	P2	P3	P4
Cross-shore	Clay	19.55	19.62	19.55	19.37
	Silt	80.40	80.28	80.28	80.38
	Sand	0.05	0.10	0.17	0.25
Alongshore	Clay	23.38	22.45	21.50	17.90
	Silt	76.57	77.50	78.43	81.94
	Sand	0.06	0.05	0.06	0.16

Table 4
Net sediment transport rate proportion of each fraction at −2.5 m.

Low water line	Sediment ID	Transport rate proportion (%)			
		P1	P2	P3	P4
Cross-shore	Clay	18.77	18.38	17.01	17.11
	Silt	80.59	81.02	82.21	81.78
	Sand	0.64	0.60	0.78	1.11
Alongshore	Clay	21.40	21.34	19.68	18.46
	Silt	78.16	78.30	79.95	80.93
	Sand	0.44	0.36	0.37	0.61

This variation pattern suggests the north profiles tend to be coarser while the south ones tend to be finer, which is totally opposite to our observations.

With the same initial bed composition setting, we cannot derive the observed southward coarsening pattern under the alongshore hydrodynamic variation. Apparently, the hydrodynamics alongshore gradient are not the main mechanism leading to the alongshore sediment grain size distribution pattern on the Jiangsu Coast. We further discuss the mechanism behind this phenomenon in Section 4.3.

3.3. Comparison between the different initial bed composition settings

Since we consider the alongshore variations in morphology and sedimentology are determined by the alongshore gradient in

hydrodynamic forcing, we applied the same initial bed sediment compositions for all the four sections in the previous simulations. It turns out that neither the derived shoreline evolution nor alongshore sediment grain size distribution pattern matches the measured ones. In order to arrive at a good match, we take the variation of initial bed material composition into consideration in the following simulations. In the previous field data study (Kuai et al., 2021), we have the bed sediment samples data about every 500 m along each measured profile (Fig. 1). In the following simulation, we linearly interpolate the proportion of sand, silt and clay from landward end to seaward end in the model domain (Table 5) according to this measured dataset.

We compare the simulated net sediment transport rate between the initial varying and constant bed composition runs. As the sand transport proportion is quite small compared to the clay and silt fraction (about 1–2 orders smaller than the other two fractions, see Tables 3 and 4), we only present the difference of the clay and silt transport rate between different transects (Fig. 9). As it can be seen from the figure, the initial bed composition does have a great impact on the net sediment transport pattern. There is a remarkable difference of the relative net sediment transport magnitude between these two bed composition settings between the P2 and P3. By considering the bed composition variation, we get a slightly decreasing trend of the net alongshore sediment transport rate between P2 and P3, which matches well with the measured mild sedimentation condition in this part of the coast. In the bed composition variation run, the initial bed composition reflects the southward coarsening pattern between P2 and P4, which is more obvious between P2 and P3 (Table 5). Due to the increase in sand composition and decrease in silt and clay compositions from P2 to P3, the net total sediment transport rate decreases as well. Sand particles are more difficult to start into motion as compared to silt and clay, and silt and clay have a larger net transport rate due to the scour and settling lag effect.

The relative net sediment transport magnitudes between P1 and P2, P3 and P4 are similar in these two bed composition settings. Considering the bed composition variation, we find that cross-shore transport rate between P2 and P4 has minor difference, which further indicated that it is mainly alongshore gradient in alongshore sediment transport rate leading to the shoreline erosion/sedimentation evolution on this coast.

As a conclusion, the alongshore gradient in hydrodynamic forcing is not the only mechanism forming the alongshore morphology variation, especially for the erosion/sedimentation (P2 and P3) transition part of the coast. The bed sediment composition is also a very important factor in determining the shoreline evolution condition. We can only derive the right shoreline evolution pattern by applying the bed composition variation in the simulation. It is very important to take the bed composition into consideration, if we want to reproduce large spatial scale shoreline evolution condition with numerical model.

4. Discussions

4.1. Sensitivity test of the SSC boundary condition

In our models we apply the same SSC boundaries for different scenarios. In reality, the yearly mean SSC is different at different alongshore locations, and its cross-shore distribution and composition are varying as well. These are influenced by many factors, like the large-scale, non-equilibrium background sediment supply, local topography and hydrodynamics. In our study we only investigate the sediment transport pattern in the middle profile of the model, and make the model domain large enough to eliminate the influence from the boundary SSC condition. The adaptation length-scale of the SSC (viz. the influenced distance by the boundary) is typically defined as a function of the water depth times the flow velocity divided by the sediment settling velocity (Galappatti and Vreugdenhil, 1985). For our model settings, the adaptation length-scale of the SSC is about 5 km near the low water line, and smaller in the intertidal zone. As a result, the 10 km horizontal length is considered large enough to minimize the boundary influence and computation time.

In order to test the sensitivity of the modelled net sediment transport rate to the SSC boundary condition, we set up two extra test scenarios. The first one is the High SSC case, which takes the same SSC boundary conditions as the measured data in Dafeng, i.e. the SSC is set to decrease linearly from 1.25 kg/m^3 at the landward edge to 0.75 kg/m^3 at the seaward end. The ratio between SSC of clay and silt is 1:4. The second one is the Low SSC case, in which the SSC is only half as compared to the High SSC case, i.e. the SSC is set to decrease linearly from 0.625 kg/m^3 at the landward edge to 0.375 kg/m^3 at the seaward end. The other model settings of these two cases are the same as the Dafeng case. After letting the model run for 30 M2 tidal cycles (long enough to get the stable sediment transport in the whole model domain), we calculate the net sediment transport rate during one M2 tidal cycle along the central profile in these two cases (Fig. 10).

Fig. 10 shows that the difference in SSC boundary does influence the sediment transport rate in the offshore zones. However, its influence gradually becomes negligible when it comes to the intertidal zones (see also Table 6). The variation of net sediment transport rate is about 10 % in the low water line, which is much smaller as compared to the fluctuations in the boundary SSC with a factor of 2. On the other hand, in this study we focus on the alongshore gradient of the net sediment transport rate, and this 10 % difference is small as it compared to the alongshore difference in sediment transport rate. So we may consider the sediment transport rate in the area of interest is not sensitive to the boundary SSC condition, as long as the model domain is large enough (in our case the 10 km), and interested area is far enough from the boundary. In other words, the variation of alongshore sediment transport rates as a result of changes in the hydrodynamic forcing, beach slope and bed composition are not affected by the assumed SSC at the model boundaries.

4.2. The mechanism behind the southward coarsening pattern

We hypothesized that the southward coarsening pattern could be caused by the alongshore hydrodynamic gradient. To prove this hypothesis, we calculated the net transport rate of different sediment fractions by setting constant bed composition at different profiles. From the simulated net sediment transport pattern with constant bed composition, we can find that the relative contribution of fine sediment to the net southwards transport is larger in the north as compared to the south. This behavior can be explain by the selective erosion, transport and deposition processes. When the eroded sediments from the northern coast are transporting southwards, the coarser fractions will gradually deposit alongshore first. The finer fractions can be transported a longer distance, and finally reach further southward. Our model proves that under the alongshore gradient in hydrodynamic forcing, the north part is getting coarser while the south part is getting finer, which means there must be another mechanism leading to the observed pattern.

By focusing on the formation of the Jiangsu Coast, we find that the sediment provenance is the main mechanism behind the southward coarsening pattern. Historically, the Jiangsu Coast was mainly fed by the sediment from two large rivers, i.e. the paleo-Yangtze River during the end of the late Pleistocene (Wang et al., 1999), and the Old Yellow River in the most recent period from 1128 to 1855 CE (Gao, 2009). The sediment supplied by the paleo-Yangtze River is found coarser as

Table 5
Initial bed compositions (according to field data) for different scenarios.

Scenario ID	Bed fraction land to sea (%)		
	Sand	Silt	Clay
P1	50–80	45–20	5–0
P2	10–50	80–50	10–0
P3	35–80	60–20	5–0
P4	43–90	55–10	2–0

Table 6
Net sediment transport rate with different boundary SSC condition setting (Δ is the difference compared to the High SSC scenario).

Scenario ID	MSL				LWL			
	Cross-shore		Alongshore		Cross-shore		Alongshore	
	Q_C (m^2/s)	Δ (%)	Q_L (m^2/s)	Δ (%)	Q_C (m^2/s)	Δ (%)	Q_L (m^2/s)	Δ (%)
High SSC	−5.63E-06	0.00	−9.71E-05	0.00	−4.53E-05	0.00	−2.11E-03	0.00
Low SSC	−5.59E-06	−0.86	−9.73E-05	0.18	−4.03E-05	−10.90	−1.95E-03	−7.43

compared to the Old Yellow River (Yang et al., 2002; Wang et al., 2017). So, initially the sediment on the south part of the Jiangsu Coast was coarser than it in the north.

Nowadays, the suspended sediment along the Jiangsu Coast is mainly from the bed erosion, rather than fluvial supply (Zhou et al., 2014). According to a detailed sediment transport model study (Yao et al., 2018), the eroded sediment from the AYRD and offshore RSRs are currently the main sediment source for the nearshore zone of the Jiangsu Coast. Although the sediment sources of the RSRs are debatable (Chen et al., 2013a), some geological measurement results (e.g., Yang et al., 2002; Wang et al., 2012a) show that the RSRs have coarser materials as compared to the AYRD. From our model results, we find that the net onshore sediment transport rate near the low water line in the south profiles is larger as compared to that in the north profiles. This means the offshore RSRs continuously serve as a sediment source for the intertidal flat on the sheltered coast, and the southwards coarsening pattern can be maintained.

As a conclusion, our model proves that this southward coarsening pattern cannot be generated or maintained by the alongshore variation of the hydrodynamics, instead it is caused by the different sediment provenance, viz. the Old Yellow River and paleo-Yangtze River in the history, and the AYRD and offshore RSRs in the present.

4.3. The mechanism behind the southward flattening pattern

By looking at the conceptual figure of the Jiangsu Coast (Fig. 3), we can notice that the northern Jiangsu coast is under erosion while the southern part is still accreting. Meanwhile the transition boundary between the two parts is gradually moving southwards. This provides the evidence that this coastline is gradually transiting from eroding to accreting from north (near the AYRD) to the south (near the central region of the RSRs). In our model, we try to reproduce the history of shoreline with originally spatial uniform sediment distribution. Due to morphological changes and redistribution of sediments, we cannot get the shoreline evolution in align with the existing data. Apparently, the sediment provenance difference is very important in the shoreline evolution.

The eroding in the north part (P1 to P2) is caused by both sediment supply shortage and alongshore gradient in hydrodynamics. Due to the northward shift of the Yellow River, there is sharp decrease in the fluvial sediment supply to the AYRD. Meanwhile, as there is no sheltering outside the AYRD, waves can continuously stir up the bed materials and flow will carry them towards the south. On the other hand, the tidal amplitude is increasing from the tip of the AYRD southwards, which leads to a larger transport capacity towards the south. As a consequence, the AYRD is gradually losing its sediments. The eroded fine sediment from the north part partly transports southwards and eventually settles along the coastline.

In the erosion/sedimentation transition zone (around P2 to P3), despite the hydrodynamics is stronger to the south, the bed material is also coarser to the south due to sediment provenance difference. This means the bed sediments have more resistance to the hydrodynamic forcing, which leads to the slightly sedimentation in this zone. According to the conceptual figure, the coarser bed composition in this zone may come from the RSRs, which also serves as a sediment source for the accreting coastline.

When it comes to further south, this part of coastline (P3 to P4) is sheltered by the RSRs. The RSRs can largely shelter the coast from offshore waves, which provides the sediment a relative milder environment to settle down. As a consequence, this part is experiencing continuous sedimentation.

In the tide-dominated environment, it is a generic phenomenon that the eroding flats are steeper than the accreting ones. Given the shoreline evolution pattern from north to south, this southward flattening pattern is just consistent to the shoreline state. And our model shows that in order to get the reliable shoreline evolution simulation, it is very important to consider the spatial variation in bed sediment composition.

5. Conclusions

From previous field data study, we find a special relationship between alongshore beach slope variation and sediment grain size pattern on the intertidal flats along the Jiangsu Coast as compared to other tide-dominated muddy flats, i.e. the beach is getting milder southward while the sediment grain size is getting coarser. By formulating a conceptual figure focusing on the alongshore variation in hydrodynamic processes and shoreline evolution pattern, we consider the special phenomenon is related to the alongshore gradient in hydrodynamic forcing. After testing the hypothesis with a highly schematized 1D Delft3D numerical model, we have the following conclusions:

1. The southwards flattening pattern is consistent with the shoreline evolution pattern (i.e. erosion to accretion from north to south), and accreting coast tends to be milder.
2. The alongshore shoreline evolution pattern is not only determined by the alongshore gradient in hydrodynamic forcing, but also influenced by the alongshore variation in bed composition. In the erosion/sedimentation transition zone, the bed composition factor plays the major role.
3. The southwards coarsening pattern cannot be explained by the classical sediment transport processes under the alongshore hydrodynamic gradient. The only way to explain this phenomenon is different sediment provenances.
4. In order to make a reliable morphological simulation of the Jiangsu Coast, it is very important to take into account the effect of spatial variations in sediment composition.

Declaration of competing interest

The authors declare that they have no known competing financial interests or personal relationships that could have appeared to influence the work reported in this paper.

Data availability

Data will be made available on request.

Acknowledgements

The first author thanks the China Scholarship Council for providing the research grant. Zhenshan Xu, Peng Yao from the Hohai University, China and Qinghua Ye from the Deltares, the Netherlands, are thanked

for the kind assistance and help with the numerical model work.

References

Alexander, C.R., Nittrouer, C.A., Demaster, D.J., Park, Y.A., Park, S.C., 1991. Macrotidal mudflats of the southwestern korean coast; a model for interpretation of intertidal deposits. J. Sediment. Res. 61 (5), 805–824.

Bearman, J.A., Friedrichs, C.T., Jaffe, B.E., Foxgrover, A.C., 2010. Spatial trends in tidal flat shape and associated environmental parameters in South San Francisco Bay. J. Coast. Res. 26 (2), 342–349.

Chen, P., Sun, Z., Zhou, X., Xia, Y., Li, L., He, Z., Wang, R., Xie, H., 2021. Impacts of coastal reclamation on tidal and sediment dynamics in the Rui'an coast of China. Ocean Dyn. 71 (3), 323–341.

Chen, C., Wang, Y.G., Huang, H.M., Yuan, C.G., 2013a. Advancement in impacts of tidal dynamics on radial sand ridges (in chinese with an English abstract). Port Waterw. Eng. 8, 17–24.

Chen, Y., Xie, D., Zhang, C., Qian, X., 2013b. Estimation of long-term wave statistics in the East China Sea. J. Coast. Res. 65 (10065), 177–182.

Elfrink, B., Baldock, T., 2002. Hydrodynamics and sediment transport in the swash zone: a review and perspectives. Coast. Eng. 45 (3–4), 149–167.

Engelund, F., Hansen, E., 1967. A Monograph on Sediment Transport in Alluvial Streams. Technical University of Denmark 0stervoldgade 10, Copenhagen K.

Friedrichs, C.T., 2012. Tidal Flat Morphodynamics: A Synthesis, Treatise on Estuarine and Coastal Science. Elsevier Inc.

Galappatti, G., Vreugdenhil, C.B., 1985. A depth-integrated model for suspended sediment transport. J. Hydraul. Res. 23 (4), 359–377.

Gao, S., 2009. Modeling the preservation potential of tidal flat sedimentary records, Jiangsu coast, eastern China. Cont. Shelf Res. 29 (16), 1927–1936.

Gao, S., 2019. Geomorphology and sedimentology of tidal flats. In: Coastal Wetlands. Elsevier, pp. 359–381.

Gong, Z., Huang, S.H., Xu, B.B., Zhu, S.Y., Zhang, Y.S., Zhou, Z., 2019a. Evolution of tidal flat in response to storm surges: a case study from the Central Jiangsu Coast (in chinese with an English abstract). Adv. Water Sci. 30 (2), 243–254.

Gong, Z., Wang, Z., Stive, M.J.F., Zhang, C., Chu, A., 2012. Process-based morphodynamic modeling of a schematized mudflat dominated by a long-shore tidal current at the central Jiangsu Coast, China. J. Coast. Res. 28 (6), 1381–1392.

Gong, Z., Zhang, Y.S., Zhao, K., Zhou, Z., Zhang, C.K., 2019b. Advances in coastal storm impacts on morphological evolution of mud tidal flat-creek system (in chinese with an English abstract). Adv. Sci. Technol. Water Resour. 39 (4), 75–84.

Green, M.O., Coco, G., 2007. Sediment transport on an estuarine intertidal flat: measurements and conceptual model of waves, rainfall and exchanges with a tidal creek. Estuar. Coast. Shelf Sci. 72 (4), 553–569.

Gugliotta, M., Saito, Y., Nguyen, V.L., Ta, T.K.O., Tamura, T., 2019. Sediment distribution and depositional processes along the fluvial to marine transition zone of the Mekong River delta, Vietnam. Sedimentology 66 (1), 146–164.

Le Hir, P., Roberts, W., Cazaillet, O., Christie, M., Bassoullet, P., Bacher, C., 2000. Characterization of intertidal flat hydrodynamics. Cont. Shelf Res. 20 (12–13), 1433–1459.

Kuai, Y., Tao, J., Zhou, Z., Aarninkhof, S., Wang, Z.B., 2021. Sediment Characteristics and Intertidal Beach Slopes along the Jiangsu Coast, China. J. Mar. Sci. Eng. 9 (3), 347.

Lesser, G.R., Roelvink, J.V., van Kester, J.T.M., Stelling, G.S., 2004. Development and validation of a three-dimensional morphological model. Coast. Eng. 51 (8–9), 883–915.

Liu, X.J., Gao, S., Wang, Y.P., 2011. Modeling profile shape evolution for accreting tidal flats composed of mud and sand: a case study of the central Jiangsu coast, China. Cont. Shelf Res. 31 (16), 1750–1760.

Maan, D.C., Van Prooijen, B.C., Wang, Z.B., De Vriend, H.J., 2015. Do intertidal flats ever reach equilibrium? J. Geophys. Res. Earth Surf. 120 (11), 2406–2436.

Muller, J.R., Chan, Y.C., Piersma, T., Chen, Y.P., Aarninkhof, S.G., Hassell, C.J., Tao, J.F., Gong, Z., Wang, Z.B., van Maren, D.S., 2020. Building for nature: preserving threatened bird habitat in port design. Water 12 (8), 2134.

Partheniades, E., 1965. Erosion and deposition of cohesive soils. J. Hydraul. Div. 91 (1), 105–139.

Pritchard, D., Hogg, A.J., 2003. Cross-shore sediment transport and the equilibrium morphology of mudflats under tidal currents. J. Geophys. Res. Oceans 108 (C10).

Pritchard, D., Hogg, A.J., Roberts, W., 2002. Morphological modelling of intertidal mudflats: the role of cross-shore tidal currents. Cont. Shelf Res. 22 (11–13), 1887–1895.

Pu, J., Chen, Y., Su, M., Mei, J., Yang, X., Yu, Z., Yao, P., 2022. Residual Sediment Transport in the Fine-Grained Jiangsu Coast under changing climate: the Role of Wind-Driven Currents. Water 14 (19), 3113.

Reed, D., van Wesenbeeck, B., Herman, P.M., Meselhe, E., 2018. Tidal flat-wetland systems as flood defenses: Understanding biogeomorphic controls. Estuar. Coast. Shelf Sci. 213, 269–282.

Ren, M.E., 1986. Comprehensive investigation of the coastal zone and tidal land resources of Jiangsu Province, 5. China Ocean Press, Beijing, p. l.

Roberts, W., Le Hir, P., Whitehouse, R.J.S., 2000. Investigation using simple mathematical models of the effect of tidal currents and waves on the profile shape of intertidal mudflats. Cont. Shelf Res. 20 (10–11), 1079–1097.

Roelvink, J.A., Walstra, D.J., 2004. Keeping it simple by using complex models. Adv. Hydro-Sci. Eng. 6, 1–11.

Su, M., Yao, P., Wang, Z.B., Zhang, C.K., Stive, M.J., 2017. Exploratory morphodynamic modeling of the evolution of the Jiangsu coast, China, since 1855: Contributions of old Yellow River-derived sediment. Mar. Geol. 390, 306–320.

Tong, S.S., Deroin, J.P., Pham, T.L., 2020. An optimal waterline approach for studying tidal flat morphological changes using remote sensing data: a case of the northern coast of Vietnam. Estuar. Coast. Shelf Sci. 236, 106613.

Wang, Y., Liu, Y., Jin, S., Sun, C., Wei, X., 2019a. Evolution of the topography of tidal flats and sandbanks along the Jiangsu coast from 1973 to 2016 observed from satellites. ISPRS J. Photogramm. Remote Sens. 150, 27–43.

Wang, Y., Wang, Y.P., Yu, Q., Du, Z., Wang, Z.B., Gao, S., 2019b. Sand-mud tidal flat morphodynamics influenced by alongshore tidal currents. J. Geophys. Res. Oceans 124 (6), 3818–3836.

Wang, Y., Zhang, Y., Zou, X., Zhu, D., Piper, D., 2012a. The sand ridge field of the South Yellow Sea: origin by river–sea interaction. Mar. Geol. 291, 132–146.

Wang, Y., Zhu, D., You, K., Pan, S., Zhu, X., Zou, X., Zhang, Y., 1999. Evolution of radiative sand ridge field of the South Yellow Sea and its sedimentary characteristics. Sci. China Ser. D Earth Sci. 42 (1), 97–112.

Wang, Y.P., Gao, S., Jia, J., Thompson, C.E., Gao, J., Yang, Y., 2012b. Sediment transport over an accretional intertidal flat with influences of reclamation, Jiangsu coast, China. Mar. Geol. 291, 147–161.

Wang, L., Hu, S., Yu, G., Ma, M., Liao, M., 2017. Comparative study on magnetic minerals of tidal flat deposits from different sediment sources in Jiangsu coast, Eastern China. Stud. Geophys. Geod. 61 (4), 754–771.

Wang, Y., Gao, S., Jia, J., 2006. High-resolution data collection for analysis of sediment dynamic processes associated with combined current-wave action over intertidal flats. Chin. Sci. Bull. 51 (7), 866–877.

Whitehouse, R.J.S., Bassoullet, P., Dyer, K.R., Mitchener, H.J., Roberts, W., 2000. The influence of bedforms on flow and sediment transport over intertidal mudflats. Cont. Shelf Res. 20 (10–11), 1099–1124.

Xing, F., Wang, Y.P., Wang, H.V., 2012. Tidal hydrodynamics and fine-grained sediment transport on the radial sand ridge system in the southern Yellow Sea. Mar. Geol. 291, 192–210.

Xu, F., Tao, J., Zhou, Z., Coco, G., Zhang, C., 2016. Mechanisms underlying the regional morphological differences between the northern and southern radial sand ridges along the Jiangsu Coast, China. Mar. Geol. 371, 1–17.

Yamada, F., Kobayashi, N., 2004. Annual variations of tide level and mudflat profile. J. Waterw. Port Coast. Ocean Eng. 130 (3), 119–126.

Yang, S.Y., Li, C.X., Jung, H.S., Lee, H.J., 2002. Discrimination of geochemical compositions between the Changjiang and the Huanghe sediments and its application for the identification of sediment source in the Jiangsu coastal plain, China. Mar. Geol. 186 (3-4), 229–241.

Yao, P., Su, M., Wang, Z., van Rijn, L.C., Zhang, C., Stive, M.J., 2018. Modelling tidal-induced sediment transport in a sand-silt mixed environment from days to years: Application to the Jiangsu coastal water, China. Coast. Eng. 141, 86–106.

Zhang, R.S., Lu, L.Y., Wang, Y.H., 2002. The mechanism and trend of coastal erosion of Jiangsu Province in China (in chinese with an English abstract). Geogr. Res. 21 (4), 469–478.

Zhang, D.S., Zhang, J.L., Zhang, C.K., Wang, Z., 1998. Tidal currents develop-storm surges destroytidal currents restore–A preliminary explanation for the dynamic mechanism of formation and evolution of radiate sand ridges in Yellow Sea (in chinese with an English abstract). Sci. China. Ser. D Earth Sci. 28, 394–402.

Zhou, L., Liu, J., Saito, Y., Zhang, Z., Chu, H., Hu, G., 2014. Coastal erosion as a major sediment supplier to continental shelves: example from the abandoned Old Huanghe (Yellow River) delta. Cont. Shelf Res. 82, 43–59.

Zhou, Z., Coco, G., van der Wegen, M., Gong, Z., Zhang, C., Townend, I., 2015. Modeling sorting dynamics of cohesive and non-cohesive sediments on intertidal flats under the effect of tides and wind waves. Cont. Shelf Res. 104, 76–91.